Antonie van Leeuwenhoek (2025) 118:117
https://doi.org/10.1007/s10482-025-02120-w

ORIGINAL PAPER

Zhengella sedimenti sp. nov. and *Phycobacter sedimenti* sp. nov., two novel bacteria isolated from coastal sediment with genomic and metabolic analysis

Pei-Ran Lin · Li-Jia-Yu Deng · Han-Zhe Zhang · Le Liu · Tian-He Liu · De-Chen Lu · Zong-Jun Du

Received: 8 March 2025 / Accepted: 21 June 2025 / Published online: 19 July 2025

Abstract In this study, two novel Gram-stain-negative bacterial strains, K97^T and ZM62^T, were isolated from sediment samples collected along the coast of Weihai, China, and described using polyphasic taxonomic techniques. Phylogenetic analysis based on the 16S rRNA gene sequence revealed that strain K97^T exhibited the highest sequence similarity (98.34%) with *Phycobacter azelaicus* F10^T within the genus *Phycobacter*, followed by *Pseudooceanicola marinus* AZO-C^T (97.14%) and *Phaeobacter italicus* LMG24365^T (96.85%). Strain ZM62^T exhibited the highest sequence similarity (98.53%) with *Zhengella mangrovi* X9-2-2^T within the genus *Zhengella*, followed by *Phyllobacterium myrsinacearum* NBRC 100019^T (96.49%) and *Oricola thermophila* MEBiC13590^T (96.35%). The respiratory quinone was Q-10 for both strains. The major fatty acid in both strains K97^T and ZM62^T is Summed Feature 8 ($C_{18:1}\omega6c/C_{18:1}\omega7c$). The main polar lipids for strain K97^T included diphosphatidylglycerol (DPG), phosphatidylethanolamine (PE), and phosphatidylglycerol (PG), while for strain ZM62^T, the main polar lipids included diphosphatidylglycerol (DPG), phosphatidylglycerol (PG), phosphatidylethanolamine (PE), and phosphatidylcholine (PC). Based on the polyphasic taxonomic data, strain K97^T is proposed as a novel species within the genus *Phycobacter*, for which the name *Phycobacter sedimenti* is proposed, and the type strain is K97^T (= KCTC 8365^T = MCCC 1H01460^T). Strain ZM62^T is proposed as a novel species within the genus *Zhengella*, for which the name *Zhengella sedimenti* is proposed, and the type strain is ZM62^T (= KCTC 8813^T = MCCC 1H01495^T). Additionally, genomic and metabolic analyses revealed that the genus *Phycobacter* possesses DMSP synthesis and metabolism genes and a complete CMP-KDO pathway, indicating potential symbiosis with algae. Metabolic analysis of strain ZM62^T indicates its potential role in the degradation of xenobiotic compounds, supported by the presence of annotated pathways for aminobenzoate (ko00627) and toluene (ko00623) degradation.

Keywords *Phycobacter* · *Zhengella* · Polyphasic taxonomy · *Roseobacteraceae* · *Notoacmeibacteraceae* · Metabolic capability

Supplementary Information The online version contains supplementary material available at https://doi.org/10.1007/s10482-025-02120-w.

P.-R. Lin · L.-J. Deng · H.-Z. Zhang · T.-H. Liu · Z.-J. Du
SDU-ANU Joint Science College, Shandong University, Weihai 264209, Shandong, China

L. Liu · D.-C. Lu (✉) · Z.-J. Du (✉)
Marine College, Shandong University, Weihai 264209, Shandong, China
e-mail: DechenLu@hotmail.com

Z.-J. Du
e-mail: duzongjun@sdu.edu.cn

D.-C. Lu · Z.-J. Du
State Key Laboratory of Microbial Technology, Shandong University, Qingdao 266237, Shandong, China

Abbreviations

AAI	Amino acid identity
ANI	Average nucleotide identity
BLAST	Basic Local Alignment Search Tool
HPLC	High performance liquid chromatography
KCTC	Korean Collection for Type Cultures
MA	Marine Agar 2216 (simplified)
MB	Marine Broth 2216E (simplified)
MCCC	Marine Culture Collection of China
MEGA	Molecular Evolutionary Genetics Analysis
MIDI	Microbial identification system
dDDH	Digital DNA–DNA hybridization
DPG	Diphosphatidylglycerol
PE	Phosphatidylethanolamine
PG	Phosphatidylglycerol
PC	Phosphatidylcholine

Introduction

Roseobacteraceae are bacteria widely distributed in marine, terrestrial, and freshwater environments, exhibiting strong environmental adaptability. The diverse metabolic capabilities of *Roseobacteraceae* are likely a key factor in their broad adaptability. These metabolic capabilities include participation in sulfur, nitrogen, and carbon cycles, degradation of organic substances, and interactions with plankton and animals (Liang et al. 2021). Members of the *Roseobacteraceae* family are known for their ability to degrade dimethylsulfoniopropionate (DMSP), thereby promoting global sulfur cycling. Phytoplankton secrete DMSP and often form symbiotic relationships with *Roseobacteraceae* (Curson et al. 2011). The genus *Phycobacter* was newly discovered. As of the writing of this article, only one species, *Phycobacter azelaicus*, has been classified within this genus, with the type strain F10^T being isolated and identified from the phycosphere of *Asterionellopsis glacialis* (Coe et al. 2023). Type strain *Phycobacter azelaicus* F10^T exhibits various metabolic characteristics, including but not limited to a unique response to the secondary metabolites rosmarinic acid and azelaic acid produced by diatoms, suggesting a potential symbiotic relationship between them (Shibl et al. 2020; Fei et al. 2020).

The family *Notoacmeibacteraceae*, a relatively recently identified and understudied taxon, belongs to the class *Alphaproteobacteria* (Huang et al. 2017). *Zhengella*, a genus within this family, was newly identified in 2018 and currently comprises a single species, *Zhengella mangrovi*. This species was isolated from mangrove sediments in the Yunxiao Mangrove Nature Reserve, Fujian Province, China. It demonstrates strong adaptability to high-salinity environments and is potentially capable of degrading organic pollutants, particularly exhibiting tolerance to environments rich in contaminants such as benzo[a]pyrene (Liao et al. 2018). These characteristics suggest that members of this genus may have potential applications in environmental remediation, especially in the degradation of organic pollutants. Given its isolation from an environment enriched with complex organic contaminants, *Zhengella* species may possess adaptive metabolic potential, making them suitable candidates for environmental restoration.

In this study, two novel strains, K97^T and ZM62^T, were isolated from algae-rich coastal mudflats and subjected to a polyphasic taxonomic analysis. These species were classified under the *Zhengella* and *Phycobacter* genera, respectively. Genomic and metabolomic analyses revealed the unique properties of *Phycobacter sedimenti* in the DMSP cycle and CMP-KDO metabolic pathway. Additionally, we uncovered the ecological significance of *Zhengella sedimenti*, highlighting its potential role in microbial communities and environmental adaptation.

Materials and methods

Isolation and cultivation

In July 2021, during low tide, marine sediment samples were collected from Xiaoshi Island (122°0′27.59″ E, 37°31′37.52″ N) and Jingzi Wharf (122°0′57.25″ E, 37°31′34.74″ N), Weihai, China. These samples were then stored in a cool, sterilized indoor environment. The samples were ground and homogenized, with 1 g of the homogenate weighed and mixed with 9 ml of sterile seawater (autoclaved at 121 °C for 30 min) to achieve a 10^{-1} concentration. Through serial dilution, 10^{-2} and 10^{-3} dilutions were prepared. Subsequently, 100 µL of each dilution was spread onto simplified Marine Agar 2216 (MA) solid medium, which was prepared by supplementing 0.5% (w/v) peptone and 0.1% (w/v) yeast extract

with artificial seawater containing 0.02% $NaHCO_3$, 0.07% KCl, 0.12% $CaCl_2$, 0.23% $MgCl_2$, and 0.32% $MgSO_4$ (w/v), along with 2% agar. Media were incubated at 20 °C for 4 days. Single colonies were picked and streaked onto MA medium to isolate pure strains including strains $K97^T$ and $ZM62^T$. These strains were preserved at − 80 °C in 20% (v/v) glycerol supplemented with 1% (v/v) NaCl. Strains of $K97^T$ and $ZM62^T$ were deposited in the Korean Collection for Type Cultures (KCTC) under the designation KCTC 8365^T and KCTC 8813^T, respectively, and also deposited in the Marine Culture Collection of China (MCCC) under the designation MCCC $1H01460^T$ and MCCC $1H01495^T$ (Xu et al. 2007). The phylogenetically related reference strains, *Phycobacter azelaicus* $F10^T$ and *Zhengella mangrovi* $X9\text{-}2\text{-}2^T$ were obtained from Professor Naoto Tanaka at the NRIC (Tokyo University of Agriculture, Japan) and MCCC.

Morphological, physiological, and biochemical analysis

After 48 h of incubation at optimum temperature (33 °C) on MA medium, the morphology and physiological characteristics of strains $K97^T$ and $ZM62^T$ were analyzed. Cell morphology and size were assessed using scanning electron microscopy (SEM; SU8010, Hitachi) for strain $K97^T$ and transmission electron microscopy (TEM; HT7700, Hitachi) for strain $ZM62^T$. Gram staining was conducted with a Gram stain kit from bioMérieux. Motility was examined on soft MA medium (containing 0.3% agar), and gliding motility was assessed on microscope slides coated with MA medium containing 0.7% agar using the hanging drop method (Bowman 2000).

Strains $K97^T$ and $ZM62^T$ were cultured on MA medium at 4–45 °C (4, 10, 15, 20, 25, 28, 30, 33, 37, 40, and 45 °C) to determine their growth temperature range. Each condition was tested in triplicate, and colony formation was recorded every 12 h. Unless otherwise specified, subsequent experiments were conducted at the optimal growth temperature determined from this assay. All solid medium assays were performed by three-zone streaking of freshly cultured colonies on MA plates, and all liquid cultures were inoculated with 2% (v/v) of actively growing logarithmic-phase cells in simplified Marine Broth 2216E (MB). The impact of NaCl concentration on growth was assessed using MA medium supplemented with 0–10% (w/v) NaCl (at 0, 0.5, 1, 2, 3, 4, 5, 6, 7, 8, 9, and 10%), and colony growth was monitored every 12 h. Growth at various pH levels was tested between pH 5.5 and 9.5 (in 0.5 pH unit increments) by measuring optical density (at 600 nm wavelength) after 48 h of incubation in MB medium with the addition of specific buffers, including MES (pH 5.5 and 6.0), PIPES (pH 6.5 and 7.5), HEPES (pH 7.5 and 8.0), Tricine buffer (pH 8.5), and CAPSO (pH 9.0 and 9.5) at concentrations of 20 mM. Cultures were incubated in 100-mL Erlenmeyer flasks containing 20 mL of medium on an orbital shaker at 120 rpm.

After a 2-week incubation on MA medium in an anaerobic jar, bacterial growth was evaluated under both anaerobic (10% H_2, 10% CO_2, 80% N_2) and microaerobic (5% O_2, 10% CO_2, 85% N_2) conditions, with and without 0.1% (w/v) KNO_3. The susceptibility to antibiotics was tested on MA medium using the disk diffusion method as described earlier (Patel et al. 2011). The oxidase activity was assessed using an oxidase reagent kit (bioMérieux) following the manufacturer's instructions. Catalase activity was determined by observing bubble formation upon the addition of a drop of 3% (v/v) H_2O_2. The hydrolysis of agar, starch, carboxymethyl cellulose, alginate, casein, and Tweens (20, 40, 60, and 80), as well as nitrate reduction, were investigated on MA medium using established methods (Tindall et al. 2007).

Various physiological and biochemical tests were conducted using the API 20E, API ZYM, and API 50CH identification systems (bioMérieux), as well as Biolog Gen III microPlates, following the manufacturer's instructions. The only modification made was adjusting the salinity to 2% (w/v).

Chemotaxonomic characterization analysis

Polar lipids were analyzed via two-dimensional silica gel thin-layer chromatography, which was used to extract and separate lipids from 50 mg of lyophilized cell material (Tindall et al. 2007). Detection reagents were appropriately selected for spot identification: molybdophosphoric acid (phosphomolybdic acid reagent, 5% v/v solution in ethanol; Sigma) for total polar lipids, ninhydrin reagent (0.2% solution; Sigma) for amino lipids, Zinzadze reagent (molybdenum blue spray reagent, 1.3%; Sigma) for phospholipids, and α-naphthol reagent for glycolipids (Minnikin et al. 1984). Cultures of the strains in mid to

late exponential growth phases were harvested in MB medium at 33 °C, freeze-dried for 3 days, and subjected to fatty acid determination. Fatty acids were then extracted, methylated, and analyzed using the standard MIDI (Microbial Identification) system. Respiratory quinones were extracted and purified following the methods of Minnikin et al. (1984) and analyzed via high-performance liquid chromatography (HPLC) (Kroppenstedt 1982; Minnikin et al. 1984).

16S rRNA gene sequence and phylogenetic analysis

To determine the taxonomic status of strains K97^T and ZM62^T, the 16S rRNA gene sequence was amplified via PCR using universal primers 27 F and 1492R (Weisburg et al. 1991). The purified PCR products were ligated to the pGM-T vector (Tiangen, China) and transformed into *Escherichia coli* DH5-α cells. Sequencing of positive clones was performed by BGI (Beijing Genomics Institute) using the ABI 3730XL system. To further confirm the authenticity of the 16S rRNA gene sequence, the complete 16S rRNA gene sequence was first extracted from the draft genome using the ContEst16S tool available on EzBioCloud (https://www.ezbiocloud.net/tools/contest16s) (Lee et al. 2017). This sequence was then compared with the PCR amplification results for cross-validation. The 16S rRNA gene sequences of strains K97^T and ZM62^T have been submitted to the GenBank database, and their similarity to other sequences was calculated using BLAST on the NCBI website (https://www.ncbi.nlm.nih.gov) and the EzBioCloud server (http://www.ezbiocloud.net/) (Yoon et al. 2017b; Altschul et al. 1990). Phylogenetic trees based on 16S rRNA sequences were reconstructed using the neighbor-joining (NJ), maximum likelihood (ML), maximum parsimony (MP), and minimum evolution (ME) methods implemented in MEGA X to ensure the robustness of the phylogenetic inference (Saitou and Nei 1987; Thomas 2001; Kumar et al. 2018; Rzhetsky and Nei 1992). The stability of the topology was confirmed by performing bootstrap analysis with 1000 replicates. Phylogenomic trees were inferred using IQ-TREE with reference genome sequences retrieved from the NCBI database, and subsequently visualized using the genome tree beautification tool available on Chiplot (https://www.chiplot.online/tvbot.html) (Trifinopoulos et al. 2016).

Genome sequencing and function analysis

The genomic DNA of strains K97^T and ZM62^T was extracted using a genomic DNA extraction kit (Takara, Japan) following the manufacturer's instructions. The draft genomes of strains K97^T and ZM62^T were sequenced on the Illumina HiSeq PE150 platform at Beijing Novogene Bioinformatics Technology (Beijing, China). The genomes were assembled by first preprocessing the raw data to obtain clean reads, followed by initial assembly using SOAPdenovo (v2.04), SPAdes, and ABySS (Li et al. 2008; Simpson et al. 2009). The resulting assemblies were subsequently integrated using CISA to produce more complete genome sequences (Lin and Liao 2013). The genomes were deposited in the DDBJ/EMBL/GenBank databases. The G + C content of the whole genomes were calculated based on the assembled genome sequences using the ContEst16S tool available on EzBioCloud. This tool was also employed to assess potential contamination in the strains K97^T and ZM62^T genomes (Lee et al. 2017).

In order to assess the genomic similarity between strains K97^T, ZM62^T and other species in the trees, the ANI value was computed using an online ANI calculator available at https://www.ezbiocloud.net/tools/ani (Yoon et al. 2017a) and https://jspecies.ribohost.com/jspeciesws/ (Richter et al. 2016). The average AAI was computed using an online AAI calculator available at http://enve-omics.ce.gatech.edu/aai/ (Konstantinidis 2014). Additionally, dDDH was determined using the GGDC tool accessible at https://ggdc.dsmz.de/ggdc.php# (Meier-Kolthoff et al. 2013). The coding genes of strains K97^T and ZM62^T were predicted using the GeneMarkS software (https://exon.gatech.edu/). Gene island prediction was conducted using the IslandPath-DIMOB software (Bertelli and Brinkman 2018).

Multi-database genes annotation of genomes

To comprehensively characterize gene functions, amino acid sequences of the target organisms were aligned against several specialized databases using DIAMOND with stringent parameters (E-value < 10^{-5} and alignment coverage > 40%) (Buchfink et al. 2015). Functional classification was conducted using the Clusters of Orthologous Groups of proteins (COG) database for ortholog identification,

the Carbohydrate-Active enZymes database (CAZy) for annotation of enzymes involved in carbohydrate metabolism (Cantarel et al. 2009), the Transporter Classification Database (TCDB) for identification of membrane transport proteins, the NCBI Non-Redundant (NR) protein database for general protein function annotation, and the Pathogen-Host Interactions database (PHI-base) for detection of genes related to host–pathogen interactions (Galperin et al. 2015; Cantarel et al. 2009; Saier et al. 2016; Urban et al. 2020).

KEGG metabolic pathway analysis

KEGG-based functional annotation was performed using the KofamKOALA tool, which assigns KEGG Orthologs (KOs) to genes based on profile hidden Markov models (HMMs) and adaptive score thresholds (Aramaki et al. 2020). The annotation results were then visualized using KEGG Mapper (https://www.genome.jp/kegg/mapper.html), enabling the reconstruction of metabolic pathways for strains K97^T, ZM62^T, and their phylogenetically related taxa.

Results and discussion

Morphological, physiological and biochemical characteristics

The cells of strain K97^T are Gram-stain-negative, short rods, approximately 0.41–0.55 μm wide and 1.03–1.95 μm long, without flagella (Fig. S1). Strain K97^T exhibits gliding motility but lacks flagellar motility. Strain K97^T has a broad growth range in terms of temperature (20–40 °C), pH (5.5–9.5), and especially salt tolerance (0.5–7.0%). Strain K97^T exhibits enzymatic activities including alkaline phosphatase, esterase (C_4), esterase lipase (C_8), leucine arylamidase, and naphthol-AS-BI-phosphohydrolase. It can produce acid from D-ribose, D-tagatose, and 5-keto-D-gluconate potassium. Furthermore, the API 20E test confirms that strain K97^T metabolizes arginine, ornithine, tryptophan (TDA), gelatin, and is positive for oxidase activity. In tests for carbon source utilization, strain K97^T demonstrates growth using various individual carbon sources such as D-trehalose, D-turanose, pectin, glucuronamide, tetrazolium-violet, L-lactic acid, α-keto-glutaric acid, acetoacetic acid, and acetic acid. The cells of strain ZM62^T are Gram-stain-negative, rods, approximately 1.0–1.5 μm wide and 2.0–4.0 μm long, without flagella (Fig. S1). Strain ZM62^T exhibits gliding motility. It displays broad salinity tolerance (0–8.0%, optimum 2.0%), but shows moderate adaptability to temperature (20–37 °C, optimum 30–35 °C) and pH (5.5–8.5, optimum 7.5). Strain ZM62^T exhibits enzymatic activities including alkaline phosphatase, esterase (C4), leucine arylamidase, valine arylamidase, cystine arylamidase, trypsin, α-chymotrypsin, acid phosphatase, and naphthol-AS-BI-phosphohydrolase. It can produce acid from D-ribose, D-fructose, D-tagatose, L-sorbose and potassium 5-ketogluconate. Furthermore, the API 20E test confirms that strain ZM62^T metabolizes gelatin. In tests for carbon source utilization, strain ZM62^T demonstrates growth using various individual carbon sources such as dextrin, D-trehalose, D-cellobiose, α-D-lactose, α-D-glucose.

Antibiotic sensitivity testing (10 μg/disc) of strain K97^T revealed the following inhibition zone diameters (mm): streptomycin (13), ampicillin (0), ofloxacin (17), ceftriaxone (14), norfloxacin (12), penicillin (0), carbenicillin (0), tetracycline (8), vancomycin (20), neomycin (15), clarithromycin (42), tobramycin (8), kanamycin (9), polymyxin (18), gentamicin (8), cefotaxime (13), rifampicin (20; with a fuzzy margin), lincomycin (8), erythromycin (33), and chloramphenicol (17). For strain ZM62^T, the inhibition zones (mm) were as follows: streptomycin (7), ampicillin (30), ofloxacin (4), ceftriaxone (28), norfloxacin (0), penicillin (13), carbenicillin (34), tetracycline (8), vancomycin (17), neomycin (7), clarithromycin (27), tobramycin (15), kanamycin (9), polymyxin (0), gentamicin (12), cefotaxime (15), rifampicin (20), lincomycin (0), erythromycin (23), and chloramphenicol (25).

Phylogenetic and phylogenomic analyses

The complete assembled genome sequence of strain K97^T has a total length of 4,076,839 base pairs (bp), encompassing 3,882 genes with a total gene length of 3,624,549 bp. The G + C content is 61.71 mol%. There are 237 genes longer than or equal to 2000 bp, 11 genomic islands (GIs), 62 minisatellite DNA sequences, 3 microsatellite DNA sequences, and a total of 51 non-coding RNAs (ncRNAs). The complete genome sequence of strain ZM62^T has a total

length of 3,994,773 base pairs (bp), encompassing 3,835 genes with a total gene length of 3,534,882 bp. The G+C content is 64.76 mol%. There are 205 genes longer than or equal to 2000 bp, 11 genomic islands (GIs), 63 minisatellite DNA sequences, 2 microsatellite DNA sequences, and a total of 67 non-coding RNAs (ncRNAs).

The full-length 16S rRNA gene sequence of strain K97^T (1463 bp) was extracted from the assembled genome. BLAST alignment in NCBI revealed that strain K97^T had the highest similarity with *Phycobacter azelaicus* F10^T (98.34%) and *Pseudooceanicola marinus* AZO-C^T (97.14%), with *Phycobacter azelaicus* F10^T being the most similar type species within the genus *Phycobacter*. The full-length 16S rRNA gene sequence of strain ZM62^T (1375 bp) was extracted from the assembled genome. BLAST alignment in NCBI revealed that strain ZM62^T had the highest similarity with *Zhengella mangrovi* X9-2-2^T (98.53%) and *Phyllobacterium myrsinacearum* NBRC 100019^T (97.14%), with *Zhengella mangrovi* X9-2-2^T being the most similar type species within the genus *Zhengella* (Table 1).

Based on the neighbor-joining (NJ), maximum parsimony (MP), maximum likelihood (ML), and minimum evolution (ME) methods, phylogenetic trees of 16S rRNA gene sequences were constructed for strains K97^T, ZM62^T, and their phylogenetically related taxa (Fig. 1, Fig. S11). All four tree-building methods consistently showed that strains K97^T and

Table 1 Differential phenotypic characteristics of strains K97^T, ZM62^T and the type strains of related species F10^T, X9-2-2^T

Characteristics	1	2	3	4
Source material	Coastal sediment	Diatom*	Coastal sediment	Mangrove sediment*
G+C content (mol%)	61.71	60*	64.76	64.9*
Cell shape	Short rods	Ovoid rod*	Rod shape	Rod shape*
Cell size (μm)	0.41–0.55×1.03–1.95	0.5–0.7×0.9–1.3*	2.0–4.0×1.0–1.5	1.5–3.0×0.8–1.1*
pH range for growth	5.5–9.5 (7–8.5)	6.0–9.6 (8.5)*	5.5–8.5 (7.5)	4–10 (7)*
NaCl range (%)	0.5–7.0 (2)	0.0–8.0 (2.0–4.0)*	0–8.0 (2.0)	0.5–7.0 (2.0)*
Growth temperature (°C)	20–40 (33–35)	22–40 (37)*	20–37 (30–35)	15–40 (30–37)*
Nitrate reduction	−	−*	+	+*
Enzyme activity				
Trypsin	+	−	+	w*
α-Chymotrypsin	−	−	w	w*
Acid phosphatase	+	−	+	+*
Naphthol-AS-BI-phosphohydrolase	−	+	+	w*
α-Galactosidase	−	−	−	−*
Utilization of selected sole carbon sources				
Glycerol	w	w	−	/
Erythritol	−	−	+	/
D-arabinose	w	w	−	/
L-arabinose	−	w	−	w*
D-Ribose	+	−	+	/
L-serine	−	+	−	/
Lincomycin	++	−	+	/
Pectin	+	−	−	/
D-galacturonic acid	−	−	−	/
Glucuronamide	+	−	+	/
Mucic acid	−	−	−	/
Tetrazolium-violet	+	+	w	/

Strains: 1, K97^T; 2, F10T, 3, ZM62^T, 4, X9-2-2^T. +, positive; w, weakly positive; −, negative, nd, no data. Values in parentheses indicate the optimal growth conditions for the strain under each parameter. All data were obtained from this study unless otherwise noted (*) (Liao et al. 2018; Coe et al. 2023)

ZM62^T each formed distinct branches with Phycobacter azelaicus F10^T and Zhengella mangrovi X9-2-2^T, respectively, with high bootstrap support values. Additionally, the NJ tree topology was selected to represent the combined results of the NJ, MP, and ML methods, and is presented in Fig. 1. A genome-based phylogenetic tree was also constructed (Fig. 2), which further supported the taxonomic placements of strains K97^T and ZM62^T.

Phylogenomic analysis based on core genome sequences revealed the distinct and well-supported phylogenetic placements of strains K97^T and ZM62^T. In the genome tree, strain K97^T formed a robust monophyletic lineage with *Phycobacter azelaicus* F10^T within the *Phycobacter* clade, clearly separated from other closely related genera such as *Leisingera*, *Phaeobacter*, and *Shimia* (Fig. 2A). Similarly, strain ZM62^T clustered tightly with *Zhengella mangrovi* X9-2-2^T, forming a distinct branch that was phylogenetically distant from members of the genera *Phyllobacterium*, *Chelativorans*, and *Nitratireductor* (Fig. 2B). To further clarify their taxonomic positions, whole-genome relatedness indices were calculated. For strain K97^T, the 16S rRNA gene sequence similarity to *Phycobacter azelaicus* NRIC 2002^T was below the commonly accepted species threshold of 98.65%, and the average nucleotide identity (ANI), average amino acid identity (AAI), and digital DNA-DNA hybridization (dDDH) values were 86.3%, 92.0%, and 30.3%, respectively. Strain ZM62^T exhibited the highest similarity to *Zhengella mangrovi* X9-2-2^T, with ANI, AAI, and dDDH values of 81.6%, 83.3%, and 23.8%, respectively. All values were markedly lower than the species delineation thresholds (ANI ≥ 95%, dDDH ≥ 70%) (Table 2). Taken together, these phylogenomic and genomic data, in combination with phenotypic and chemotaxonomic characteristics, support the classification of strain K97^T as *Phycobacter sedimenti* sp. nov. and strain ZM62^T as *Zhengella sedimenti* sp. nov.

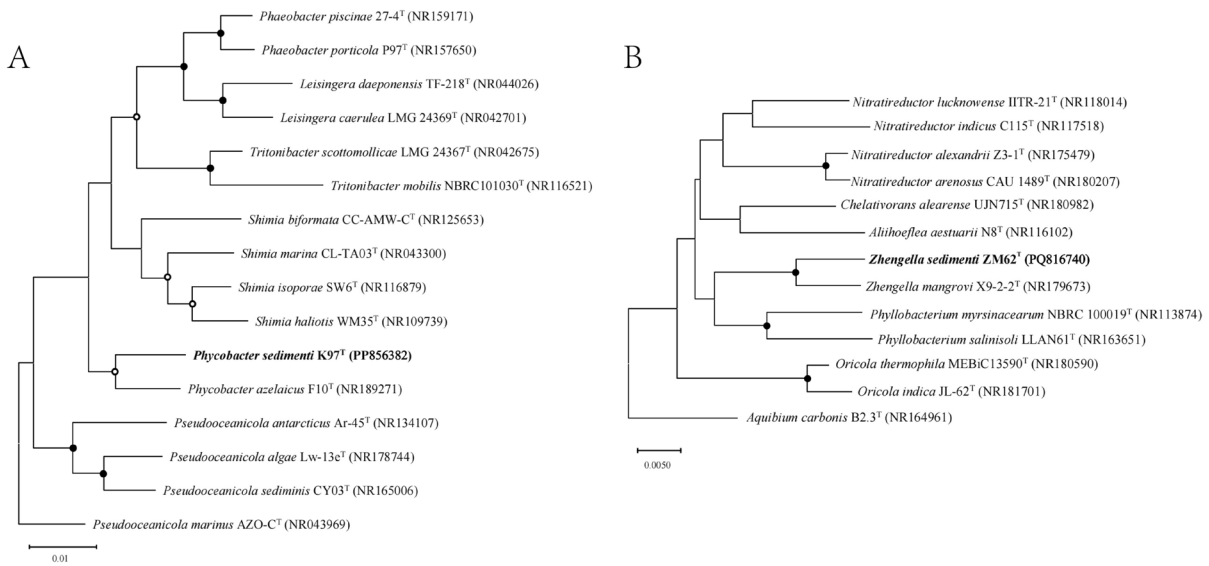

Fig. 1 The phylogenetic tree based on the 16S rRNA gene sequences of strains K97^T, ZM62^T and related taxa are shown in Fig. 1. All type strains have been included. Bootstrap values based on 1000 replicates (> 70%) are indicated at the branch nodes (ML/NJ/MP) (Saitou and Nei 1987; Felsenstein 1985; Thomas 2001). Solid circles indicate bootstrap support > 70% in all three trees; open circles indicate support in two trees. Bacteria of the *Pseudooceanicola marinus* (GenBank accession number NR043969) and *Aquibium carbonis* B2.3^T (GenBank accession number NR164961) were used as outgroups. The scale bar represents 0.01 substitutions per nucleotide position in tree A and 0.005 substitutions per nucleotide position in tree B. (Original ML/NJ/MP/ME trees are provided in Fig. S11.)

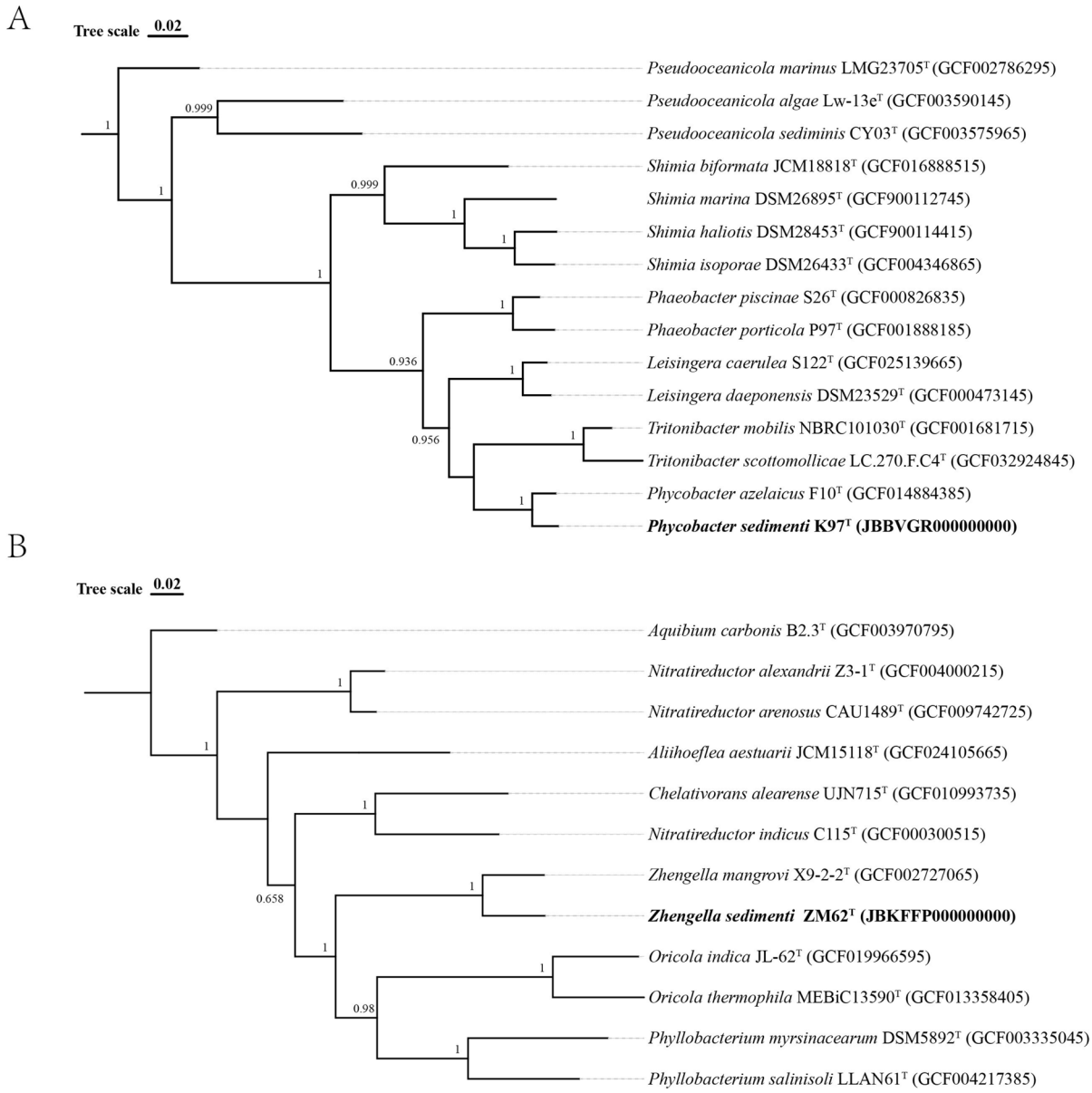

Fig. 2 Phylogenetic tree landscaping is performed using chiplot software for phylogenetic tree mapping of strains K97^T and ZM62^T (Xie et al. 2023). *Pseudooceanicola antarcticus* Ar-45^T (GCF_002786285.1) and *Aliihoeflea aestuarii* JCM 15118^T (GCF_024105665.1) were used as outgroups. Bar indicates substitutions per nucleotide site

Multi-database genes annotation of strains K97^T and ZM62^T

Multi-database annotation (KEGG, TCDB, CAZy, PHI, NR, COG) comprehensively reveals information on the metabolic capabilities, biosynthetic pathways, signal transduction, membrane transport systems, carbohydrate enzyme activity, pathogen-host interactions, and gene and protein functions of strains K97^T and ZM62^T. Notably, genes in strain K97T associated with DMSP are annotated as dimethylsulfoniopropionate demethylase, which plays an important role in energy and sulfur metabolism (KEGG). Additionally, several genes are potentially involved in glycine

Table 2 Comparison of ANI, AAI and dDDH values of reference strains against strains K97^T (top) and ZM62^T (bottom)

Strain name and number	Accession no	ANI (%)	AAI (%)	dDDH (%)
***Phycobacter sedimenti* K97^T**	**JBBVGR000000000.1**	**100**	**100**	**100**
Phycobacter azelaicus NRIC2002^T	GCF_014884385.1	86.3	92	30.3
Shimia isoporae DSM26433^T	GCF_004346865.1	76	70.1	20.2
Pseudooceanicola algae Lw-13e^T	GCF_003590145.2	72.5	67.2	19.7
Pseudooceanicola sediminis CY03^T	GCF_003575965.1	72.56	68	20
Pseudooceanicola marinus LMG23705^T	GCF_002786295.1	73	67.5	20.5
Tritonibacter scottomollicae LC.270.F.C4^T	GCF_032924845.1	75.6	75.4	20.4
Shimia marina DSM26895^T	GCF_900112745.1	72.4	70	20.4
Shimia biformata JCM18818^T	GCF_016888515.1	73.5	70.4	20.4
Tritonibacter mobilis NBRC101030^T	GCF_001681715.1	74.9	75.8	20.3
Shimia haliotis DSM28453^T	GCF_900114415.1	72.3	70	20.5
Phaeobacter piscinae S26^T	GCF_000826835.2	76	77.9	20.6
Phaeobacter porticola P97^T	GCF_001888185.1	75.3	77.47	19.7
Pseudooceanicola antarcticus Ar-45^T	GCF_002786285.1	73.24	67.68	20.4
Leisingera daeponensis DSM23529^T	GCF_000473145.1	77.58	78.69	21.4
Leisingera caerulea S122^T	GCF_025139665.1	77.4	78.63	20.9
Strain name and number	Accession no	ANI (%)	AAI (%)	dDDH (%)
***Zhengella sedimenti* ZM62^T**	**JBKFFP000000000.1**	**100**	**100**	**100**
Zhengella mangrovi X9-2-2^T	GCF_002727065.1	81.57	83.29	23.8
Aliihoeflea aestuarii JCM15118^T	GCF_024105665.1	74.69	64.03	19.6
Aquibium carbonis B2.3^T	GCF_003970795.1	75.08	66.02	19.6
Chelativorans alearense UJN715^T	GCF_010993735.1	75.94	67.86	19.6
Nitratireductor alexandrii Z3-1^T	GCF_004000215.1	75.2	67.17	19.5
Nitratireductor arenosus CAU1489^T	GCF_009742725.1	74.16	64.07	21.3
Nitratireductor indicus C115^T	GCF_000300515.1	74.35	65.92	19.9
Oricola indica JL-62^T	GCF_019966595.1	74.83	64.51	19.6
Oricola thermophila MEBiC13590^T	GCF_013358405.1	74.71	65.54	20.1
Phyllobacterium myrsinacearum DSM5892^T	GCF_004217385.1	75.07	66.59	18.8
Phyllobacterium salinisoli LLAN61^T	GCF_003335045.1	74.76	64.43	19.8

degradation and transport processes, as indicated by COG annotations. Two genes associated with acyl-homoserine lactone (AHL) are annotated as AHL acylase. One of them belongs to the penicillin acylase family, according to NR annotation, and is associated with the biosynthesis of penicillin and cephalosporin, which may explain bacterial resistance to penicillin.

Furthermore, genes involved in the synthesis, transport, and degradation of secondary metabolites were identified (COG), with KEGG annotation indicating a role in penicillin and cephalosporin biosynthesis. Multiple database annotations show that the acyl-homoserine-lactone synthase gene is also present in both strains NRIC 2002^T and K97^T. NR, SwissProt, and COG annotations for strain K97^T indicate that it possesses AHL synthase (K18096). This enzyme helps bacteria perform quorum sensing by synthesizing AHL, thereby regulating group behaviors, including but not limited to biofilm formation, virulence factor expression, and antibiotic production (Schaefer et al. 2008). For strain ZM62^T, numerous genes associated with xenobiotics biodegradation and metabolism were identified, including those involved in aminobenzoate degradation (ko00627) and toluene degradation (ko00623), suggesting its potential role in the breakdown of environmental pollutants. All this information can be found in Fig. 3 and the supplementary materials Fig. S3-S10.

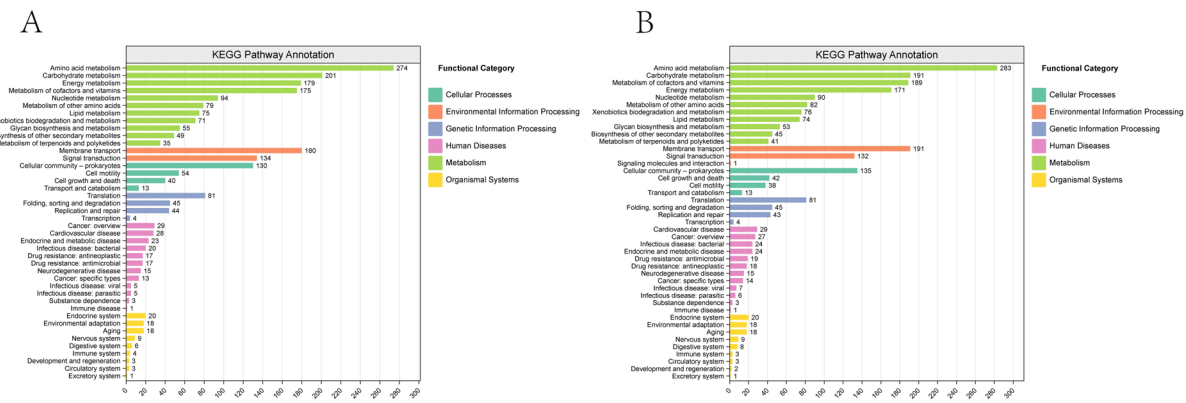

Fig. 3 The pathways of different genes of strains K97^T (**A**) and ZM62^T (**B**) were annotated and classified using KEGG database

KEGG metabolic pathway analysis of strain K97^T

Metabolic pathway reconstruction based on KEGG Mapper shows that strains K97^T and F10^T possess multiple complete metabolic pathways among the 16 strains in the phylogenetic tree, suggesting the metabolic characteristics of the genus Phycobacter (Fig. 5).

Both strains K97^T and F10^T have complete pathways for carbohydrate metabolism, energy metabolism, lipid metabolism, glycan metabolism, metabolism of cofactors and vitamins, and biosynthesis of terpenoids and polyketides. Specifically, strains K97^T and F10^T have glycolysis and 5-Phosphoribosyl-1-pyrophosphate (PRPP) biosynthesis as part of carbohydrate metabolism. In terms of energy metabolism, both strains possess complete pathways for thiosulfate oxidation by the SOX complex, cytochrome bc1 complex respiratory unit, cytochrome c oxidase (prokaryotes), cytochrome c oxidase (cbb3-type), and NADH:quinone oxidoreductase. However, only F10^T has the anoxygenic photosystem II pathway related to photosynthesis, while only strain K97^T has the reductive pentose phosphate cycle (Calvin cycle) (Fig. 4). These differences suggest that F10^T partially relies on anoxygenic photosynthesis for energy acquisition, whereas strain K97^T utilizes the Calvin cycle for carbon fixation, indicating distinct ecological adaptation strategies between the two strains.

Regarding lipid metabolism, both strains K97^T and F10^T have pathways for fatty acid biosynthesis, beta-oxidation, phosphatidylethanolamine (PE) biosynthesis, and phosphatidylcholine (PC) biosynthesis, which is consistent with our experimental results (Table 3, Fig. S2). Additionally, both strains K97^T and F10^T share a complete Cytidine Monophosphate-3-deoxy-D-manno-octulosonate (CMP-KDO) biosynthesis pathway. Among the strains in the phylogenetic tree, this pathway is detected exclusively in K97^T and F10^T, which may indicate a unique metabolic feature shared by them.

Furthermore, in the metabolism of cofactors and vitamins, strains K97^T and F10^T have complete pathways for NAD biosynthesis, coenzyme A biosynthesis, lipoic acid biosynthesis, tetrahydrofolate biosynthesis, and cobalamin biosynthesis. Finally, strain K97^T uniquely possesses the dTDP-L-rhamnose biosynthesis pathway. This suggests that both strains have strong cofactor biosynthesis capabilities, while strain K97^T may have a unique advantage in cell wall or surface structure modification (Li et al. 2022).

Compared to other bacteria in the phylogenetic tree, strains K97^T and F10^T exhibit significant differences in the biosynthesis of terpenoids and polyketides, as well as glycan metabolism. The CMP-KDO biosynthesis pathway is particularly notable. CMP-KDO is an activated sugar donor essential in bacteria like *Escherichia coli* and other Gram-stain-negative bacteria for the synthesis of a key component of lipopolysaccharide (LPS) (Sugai et al. 1995). LPS is an essential component of the outer membrane in Gram-stain-negative bacteria, providing protection against physical, chemical, and biological factors, such as antibiotics, toxins, and attacks from the host's immune system (Schaefer et al. 2008; Zhang et al. 2013; Tsujimoto et al. 1999). CMP-KDO can

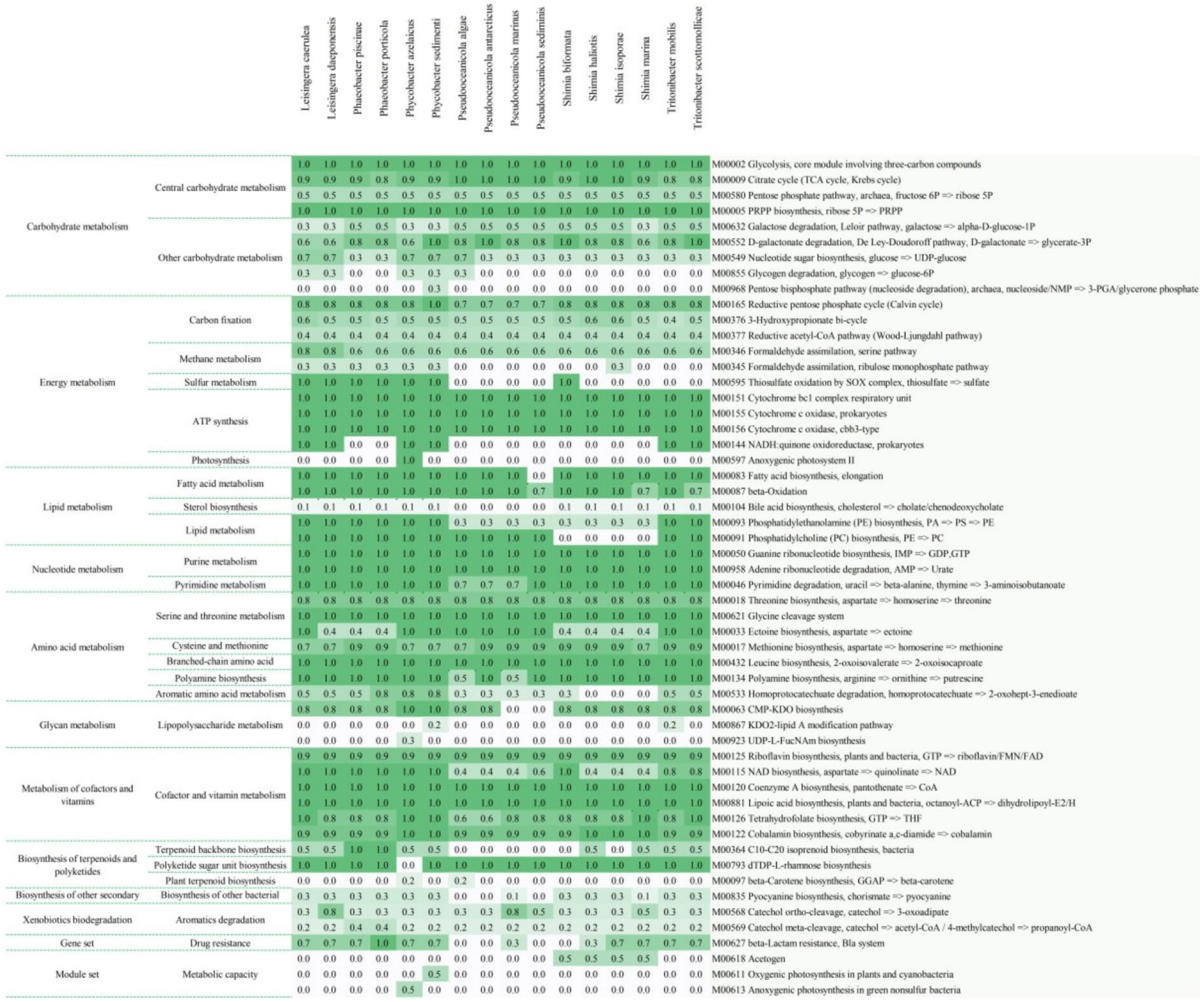

Fig. 4 The KEGG annotation diagrams for strains K97^T, NRIC 2002^T, and 14 closely related taxa in the phylogenetic tree. The numbers in the table represent the completeness of each metabolic step (1 = 100%)

also serve as an alternative sugar donor to synthesize a rare sugar, KDO-lactose (Drouillard et al. 2010; Sugai et al. 1995). Both strains K97^T and F10^T possess a complete metabolic pathway for this process, which is detailed in Fig. 4. Further research reveals that, apart from *Pseudooceanicola marinus* and *Pseudooceanicola sediminis*, the other 14 strains lack a complete CMP-KDO biosynthesis pathway due to the absence of KDO 8-P phosphatase [EC:3.1.3.45]. This enzyme is involved in lipopolysaccharide biosynthesis, metabolic pathways, and the biosynthesis of nucleotide sugars (Ray and Benedict 1980). Therefore, the absence of KDO 8-P phosphatase likely affects the typical KDO-containing LPS core synthesis but does not rule out the presence of modified LPS or other outer membrane structures.

KEGG annotation also revealed that both strains K97^T and F10^T possess the dimethylsulfoniopropionate demethylase gene [EC:2.1.1.269](*DmdA*), while most other related taxa lack this capability (Jansen and Hansen 1997). The DmdA enzyme can degrade DMSP into methylmercaptopropionate (MMPA) and methanethiol (MT), allowing bacteria to obtain energy and carbon sources in the process (Curson et al. 2011). F10^T was isolated from diatoms, which can produce DMSP and thus form a symbiotic relationship with F10^T. Similarly, strain K97^T, which also contains the DmdA gene, was isolated from

Table 3 Distinctive features of strains K97^T (1), ZM62^T (3) compared to their closely associated species F10^T (2) and X9-2-2T (4)

Fatty acid	1	2	3	4
Saturated				
$C_{12:0}$	0.59	0.74	tr	tr
$C_{16:0}$	**7.79**	**8.58**	2.72	**6.93**
$C_{17:0}$	1.25	0.92	**19.31**	**6.56**
$C_{18:0}$	**3.19**	**4.27**	2.38	1.81
Unsaturated				
$C_{15:1}\omega 5c$	0.51	tr	tr	tr
$C_{17:1}\omega 8c$	tr	tr	**4.14**	2.3
$C_{18:1}$ $\omega 7c$ 11-methyl	tr	**4.36**	tr	tr
Branched				
iso-$C_{17:0}$	tr	tr	1.55	**10.44**
iso-$C_{18:0}$	tr	1.01	tr	tr
Hydroxy				
$C_{10:1}$ 3-OH	2	2.83	tr	tr
$C_{12:0}$ 3-OH	2.05	3.35	tr	tr
$C_{16:0}$ 2-OH	**3.16**	**5.52**	tr	tr
$C_{18:1}$ 2-OH	tr	0.99	tr	tr
*Summed feature**				
$C_{16:1}$ $\omega 7c$/$C_{16:1}$ $\omega 6c$			0.52	0.81
$C_{19:1}$ $\omega 7c$/$C_{19:1}$ $\omega 6c$	0.63	1.43	0.73	tr
$C_{18:1}$ $\omega 7c$	**75.73**	**60.01**	**47.29**	**41.33**

Summed Feature 3, Summed Feature 7, and Summed Feature 8 correspond to $C_{16:1}\omega 7c$/$C_{16:1}\omega 6c$, $C_{19:1}$ $\omega 7c$/$C_{19:1}$ $\omega 6c$, and $C_{18:1}$ $\omega 7c$, respectively. 'tr' (trace) indicates that the detected proportion of the fatty acid is less than 0.5%. Values in bold indicate fatty acid contents greater than 5%

nearshore sediments rich in algae, and it may also have the potential to form a symbiotic relationship with algae, although this requires experimental validation (Figs. 4, 6). In summary, the ability of strains K97^T and F10^T to degrade algal-derived DMSP, combined with their broad metabolic capacities, may help reduce DMSP accumulation and mitigate its potential toxicity, thereby promoting algal stability and resilience. This suggests a potentially beneficial ecological interaction, although further experimental validation is required.

KEGG metabolic pathway analysis of strain ZM62^T

Metabolic pathway reconstruction for strain ZM62^T, performed using KEGG Mapper based on genomic annotations, reveals the presence of several significant metabolic pathways among the analyzed strains (Fig. 5B). Strain ZM62^T exhibits remarkable metabolic versatility, particularly in its ability to process various organic compounds and potentially degrade pollutants.

One of the key aspects of its metabolic capabilities is its involvement in carbohydrate metabolism, including pathways for the semi-phosphorylative Entner-Doudoroff pathway and the degradation of polygalacturonan via D-galacturonate catabolism (Zhu et al. 2017; Martens-Uzunova and Schaap 2008). These pathways enable the breakdown of complex sugars and organic acids into fundamental metabolic intermediates, supporting both energy generation and biosynthesis. Notably, its ability to metabolize D-galacturonate to pyruvate and D-glyceraldehyde-3P suggests a potential role in utilizing plant-derived polysaccharides, particularly pectin, which is enzymatically degraded into D-galacturonate by pectinolytic enzymes such as polygalacturonases and pectin lyases (Yew Wen and Gerlt John 2002). Additionally, strain ZM62^T demonstrates glycogen biosynthesis and degradation, allowing it to store and mobilize energy reserves efficiently under fluctuating environmental conditions.

In energy metabolism, strain ZM62^T harnesses the SOX-dependent thiosulfate oxidation pathway as a key mechanism in sulfur compound metabolism (Falkenby et al. 2011). This suggests an adaptation to sulfur-rich environments and a potential role in biogeochemical cycling. Furthermore, its cytochrome c oxidase (cbb3-type) respiratory pathway enhances its ability to sustain efficient electron transport processes, enabling survival in various redox conditions, including potentially oxygen-limited environments (Wu et al. 2021; Pitcher and Watmough 2004). The strain's amino acid metabolism includes unique pathways for methionine biosynthesis (aspartate → methionine) and cysteine biosynthesis (serine → cysteine). These biosynthetic routes are essential for protein synthesis and cellular function and may enable strain ZM62^T to survive in nutrient-limited environments where these amino acids are scarce.

A notable feature is the lipid metabolism of strain ZM62^T, which is equipped for phosphatidylethanolamine (PE) biosynthesis via the pathway phosphatidic acid (PA) → phosphatidylserine (PS) → phosphatidylethanolamine (PE). This finding is consistent with the results of our polar lipid experiment, and

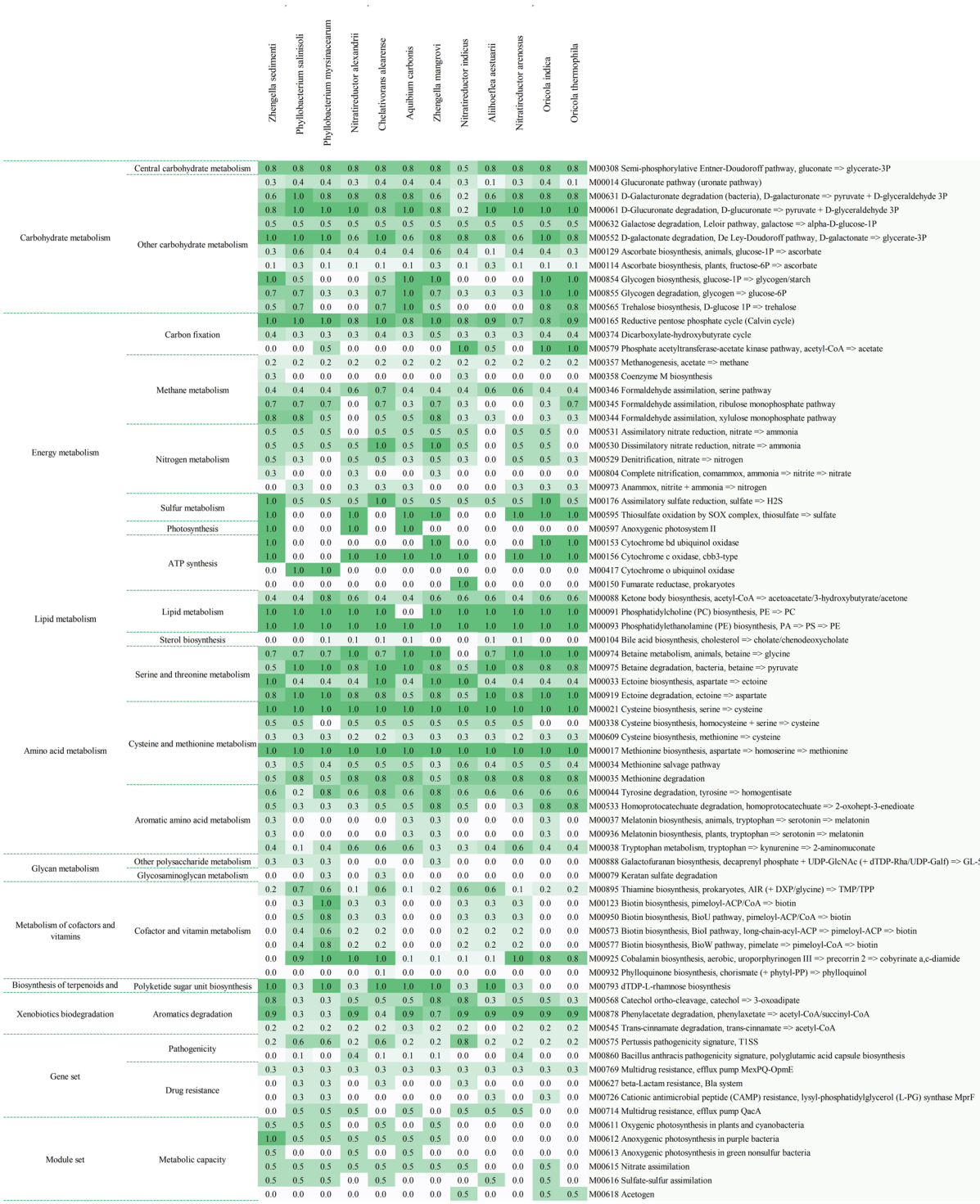

		Zhengella sediminti	Phyllobacterium salinisoli	Phyllobacterium myrsinacearum	Nitratireductor alexandrii	Chelativorans alearense	Aquibium carbonis	Zhengella mangrovi	Nitratireductor indicus	Aliihoeflea aestuarii	Nitratireductor arenosus	Oricola indica	Oricola thermophila	
Carbohydrate metabolism	Central carbohydrate metabolism	0.8	0.8	0.8	0.8	0.8	0.8	0.8	0.5	0.8	0.8	0.8	0.8	M00308 Semi-phosphorylative Entner-Doudoroff pathway, gluconate => glycerate-3P
	Other carbohydrate metabolism	0.3	0.4	0.4	0.3	0.4	0.4	0.4	0.3	0.1	0.3	0.4	0.1	M00014 Glucuronate pathway (uronate pathway)
		0.6	1.0	0.8	0.8	0.8	0.8	0.6	0.2	0.6	0.8	0.8	0.8	M00631 D-Galacturonate degradation (bacteria), D-galacturonate => pyruvate + D-glyceraldehyde 3P
		0.8	1.0	1.0	1.0	0.8	1.0	0.8	0.2	1.0	1.0	1.0	1.0	M00061 D-Glucuronate degradation, D-glucuronate => pyruvate + D-glyceraldehyde 3P
		0.5	0.5	0.5	0.5	0.5	0.5	0.5	0.5	0.5	0.5	0.5	0.5	M00632 Galactose degradation, Leloir pathway, galactose => alpha-D-glucose-1P
		1.0	1.0	1.0	0.6	1.0	0.6	0.8	0.8	0.8	0.6	1.0	0.8	M00552 D-galactonate degradation, De Ley-Doudoroff pathway, D-galactonate => glycerate-3P
		0.3	0.6	0.4	0.4	0.4	0.4	0.6	0.4	0.1	0.4	0.4	0.3	M00129 Ascorbate biosynthesis, animals, glucose-1P => ascorbate
		0.1	0.3	0.1	0.1	0.1	0.1	0.3	0.1	0.3	0.1	0.1	0.1	M00114 Ascorbate biosynthesis, plants, fructose-6P => ascorbate
		1.0	0.5	0.0	0.0	0.5	1.0	1.0	0.0	0.0	0.0	1.0	1.0	M00854 Glycogen biosynthesis, glucose-1P => glycogen/starch
		0.7	0.7	0.3	0.3	0.7	1.0	0.7	0.3	0.3	0.3	1.0	1.0	M00855 Glycogen degradation, glycogen => glucose-6P
		0.5	0.7	0.0	0.0	0.7	1.0	0.5	0.0	0.0	0.0	0.8	0.8	M00565 Trehalose biosynthesis, D-glucose 1P => trehalose
Energy metabolism	Carbon fixation	1.0	1.0	1.0	0.8	1.0	0.8	1.0	0.8	0.9	0.7	0.8	0.9	M00165 Reductive pentose phosphate cycle (Calvin cycle)
		0.4	0.3	0.3	0.3	0.4	0.3	0.5	0.3	0.3	0.3	0.4	0.4	M00374 Dicarboxylate-hydroxybutyrate cycle
		0.0	0.0	0.5	0.0	0.0	0.0	0.0	1.0	0.5	0.0	1.0	1.0	M00579 Phosphate acetyltransferase-acetate kinase pathway, acetyl-CoA => acetate
	Methane metabolism	0.2	0.2	0.2	0.2	0.2	0.2	0.2	0.2	0.2	0.2	0.2	0.2	M00357 Methanogenesis, acetate => methane
		0.3	0.0	0.0	0.0	0.0	0.0	0.0	0.3	0.0	0.0	0.0	0.0	M00358 Coenzyme M biosynthesis
		0.4	0.4	0.4	0.6	0.7	0.4	0.4	0.4	0.6	0.6	0.4	0.4	M00346 Formaldehyde assimilation, serine pathway
		0.7	0.7	0.7	0.0	0.7	0.3	0.7	0.3	0.0	0.0	0.3	0.7	M00345 Formaldehyde assimilation, ribulose monophosphate pathway
		0.8	0.8	0.5	0.0	0.5	0.5	0.8	0.3	0.3	0.0	0.3	0.3	M00344 Formaldehyde assimilation, xylulose monophosphate pathway
	Nitrogen metabolism	0.5	0.5	0.5	0.0	0.5	0.5	0.5	0.5	0.0	0.5	0.5	0.0	M00531 Assimilatory nitrate reduction, nitrate => ammonia
		0.5	0.5	0.5	0.5	1.0	0.5	1.0	0.5	0.0	0.5	0.5	0.0	M00530 Dissimilatory nitrate reduction, nitrate => ammonia
		0.5	0.3	0.0	0.5	0.5	0.3	0.5	0.3	0.0	0.5	0.5	0.3	M00529 Denitrification, nitrate => nitrogen
		0.3	0.0	0.0	0.3	0.0	0.0	0.3	0.0	0.0	0.0	0.0	0.0	M00804 Complete nitrification, comammox, ammonia => nitrite => nitrate
		0.0	0.3	0.0	0.3	0.3	0.3	0.0	0.0	0.0	0.3	0.3	0.3	M00973 Anammox, nitrite + ammonia => nitrogen
	Sulfur metabolism	1.0	0.5	0.5	0.5	1.0	0.5	0.5	0.5	0.5	0.5	1.0	0.5	M00176 Assimilatory sulfate reduction, sulfate => H2S
		1.0	0.0	0.0	1.0	0.0	1.0	1.0	0.0	0.0	1.0	1.0	1.0	M00595 Thiosulfate oxidation by SOX complex, thiosulfate => sulfate
	Photosynthesis	1.0	0.0	0.0	1.0	0.0	1.0	0.0	0.0	0.0	0.0	0.0	0.0	M00597 Anoxygenic photosystem II
	ATP synthesis	1.0	0.0	0.0	0.0	0.0	0.0	1.0	0.0	0.0	0.0	1.0	1.0	M00153 Cytochrome bd ubiquinol oxidase
		1.0	0.0	0.0	1.0	1.0	1.0	1.0	1.0	0.0	1.0	1.0	1.0	M00156 Cytochrome c oxidase, cbb3-type
		0.0	1.0	1.0	0.0	0.0	0.0	0.0	0.0	0.0	0.0	0.0	0.0	M00417 Cytochrome o ubiquinol oxidase
		0.0	0.0	0.0	0.0	0.0	0.0	0.0	1.0	0.0	0.0	0.0	0.0	M00150 Fumarate reductase, prokaryotes
Lipid metabolism	Lipid metabolism	0.4	0.4	0.8	0.6	0.4	0.4	0.6	0.6	0.6	0.4	0.6	0.6	M00088 Ketone body biosynthesis, acetyl-CoA => acetoacetate/3-hydroxybutyrate/acetone
		1.0	1.0	1.0	1.0	1.0	0.0	1.0	1.0	1.0	1.0	1.0	1.0	M00091 Phosphatidylcholine (PC) biosynthesis, PE => PC
		1.0	1.0	1.0	1.0	1.0	1.0	1.0	1.0	1.0	1.0	1.0	1.0	M00093 Phosphatidylethanolamine (PE) biosynthesis, PA => PS => PE
	Sterol biosynthesis	0.0	0.0	0.1	0.1	0.1	0.1	0.0	0.0	0.1	0.1	0.0	0.0	M00104 Bile acid biosynthesis, cholesterol => cholate/chenodeoxycholate
Amino acid metabolism	Serine and threonine metabolism	0.7	0.7	0.7	1.0	0.7	1.0	1.0	0.0	0.7	1.0	1.0	1.0	M00974 Betaine metabolism, animals, betaine => glycine
		0.5	1.0	1.0	0.8	1.0	1.0	0.8	0.5	1.0	0.8	0.8	0.8	M00975 Betaine degradation, bacteria, betaine => pyruvate
		1.0	0.4	0.4	0.4	1.0	0.4	1.0	1.0	0.4	0.4	0.4	0.4	M00033 Ectoine biosynthesis, aspartate => ectoine
		0.8	1.0	1.0	0.8	0.8	0.5	0.8	0.5	1.0	0.8	1.0	1.0	M00919 Ectoine degradation, ectoine => aspartate
	Cysteine and methionine metabolism	1.0	1.0	1.0	1.0	1.0	1.0	1.0	1.0	1.0	1.0	1.0	1.0	M00021 Cysteine biosynthesis, serine => cysteine
		0.5	0.5	0.0	0.5	0.5	0.5	0.5	0.5	0.5	0.5	0.0	0.0	M00338 Cysteine biosynthesis, homocysteine + serine => cysteine
		0.3	0.3	0.3	0.2	0.2	0.3	0.3	0.3	0.3	0.2	0.3	0.3	M00609 Cysteine biosynthesis, methionine => cysteine
		1.0	1.0	1.0	1.0	1.0	1.0	1.0	1.0	1.0	1.0	1.0	1.0	M00017 Methionine biosynthesis, aspartate => homoserine => methionine
		0.3	0.5	0.4	0.5	0.5	0.5	0.3	0.6	0.4	0.5	0.5	0.4	M00034 Methionine salvage pathway
		0.5	0.8	0.5	0.8	0.8	0.8	0.5	0.8	0.8	0.8	0.8	0.8	M00035 Methionine degradation
	Aromatic amino acid metabolism	0.6	0.2	0.8	0.6	0.8	0.6	0.8	0.6	0.6	0.6	0.6	0.6	M00044 Tyrosine degradation, tyrosine => homogentisate
		0.5	0.3	0.3	0.3	0.5	0.5	0.8	0.5	0.0	0.3	0.8	0.8	M00533 Homoprotocatechuate degradation, homoprotocatechuate => 2-oxohept-3-enedioate
		0.3	0.0	0.0	0.0	0.0	0.3	0.3	0.0	0.0	0.0	0.3	0.0	M00037 Melatonin biosynthesis, animals, tryptophan => serotonin => melatonin
		0.3	0.0	0.0	0.0	0.0	0.3	0.3	0.0	0.0	0.0	0.3	0.0	M00936 Melatonin biosynthesis, plants, tryptophan => serotonin => melatonin
		0.4	0.1	0.4	0.6	0.6	0.6	0.3	0.3	0.4	0.6	0.4	0.4	M00038 Tryptophan metabolism, tryptophan => kynurenine => 2-aminomuconate
Glycan metabolism	Other polysaccharide metabolism	0.3	0.3	0.3	0.0	0.0	0.0	0.3	0.0	0.0	0.0	0.0	0.0	M00888 Galactofuranan biosynthesis, decaprenyl phosphate + UDP-GlcNAc (+ dTDP-Rha/UDP-Galf) => GL-5
	Glycosaminoglycan metabolism	0.0	0.0	0.3	0.0	0.3	0.0	0.0	0.0	0.0	0.0	0.0	0.0	M00079 Keratan sulfate degradation
Metabolism of cofactors and vitamins	Cofactor and vitamin metabolism	0.2	0.7	0.6	0.1	0.6	0.1	0.2	0.6	0.6	0.1	0.2	0.2	M00895 Thiamine biosynthesis, prokaryotes, AIR (+ DXP/glycine) => TMP/TPP
		0.0	0.3	1.0	0.3	0.3	0.0	0.0	0.3	0.3	0.3	0.0	0.0	M00123 Biotin biosynthesis, pimeloyl-ACP/CoA => biotin
		0.0	0.5	0.8	0.3	0.3	0.0	0.0	0.3	0.3	0.3	0.0	0.0	M00950 Biotin biosynthesis, BioU pathway, pimeloyl-ACP/CoA => biotin
		0.0	0.4	0.6	0.2	0.2	0.0	0.0	0.2	0.2	0.2	0.0	0.0	M00573 Biotin biosynthesis, BioI pathway, long-chain-acyl-ACP => pimeloyl-ACP => biotin
		0.0	0.4	0.8	0.2	0.2	0.0	0.0	0.2	0.2	0.2	0.0	0.0	M00577 Biotin biosynthesis, BioW pathway, pimelate => pimeloyl-CoA => biotin
		0.0	0.9	1.0	1.0	1.0	0.1	0.1	0.1	0.1	1.0	0.8	0.8	M00925 Cobalamin biosynthesis, aerobic, uroporphyrinogen III => precorrin 2 => cobyrinate a,c-diamide
		0.0	0.0	0.0	0.0	0.1	0.0	0.0	0.0	0.0	0.0	0.0	0.0	M00932 Phylloquinone biosynthesis, chorismate (+ phytyl-PP) => phylloquinol
Biosynthesis of terpenoids and	Polyketide sugar unit biosynthesis	1.0	0.3	1.0	0.3	1.0	1.0	1.0	0.3	1.0	0.3	0.0	0.0	M00793 dTDP-L-rhamnose biosynthesis
Xenobiotics biodegradation	Aromatics degradation	0.8	0.3	0.3	0.5	0.5	0.5	0.8	0.8	0.3	0.5	0.5	0.3	M00568 Catechol ortho-cleavage, catechol => 3-oxoadipate
		0.9	0.3	0.3	0.9	0.4	0.9	0.7	0.9	0.9	0.9	0.9	0.9	M00878 Phenylacetate degradation, phenylaxetate => acetyl-CoA/succinyl-CoA
		0.2	0.2	0.2	0.2	0.2	0.3	0.2	0.2	0.0	0.2	0.2	0.2	M00545 Trans-cinnamate degradation, trans-cinnamate => acetyl-CoA
Gene set	Pathogenicity	0.2	0.6	0.6	0.2	0.6	0.2	0.2	0.8	0.2	0.2	0.2	0.2	M00575 Pertussis pathogenicity signature, T1SS
		0.0	0.1	0.0	0.4	0.1	0.1	0.1	0.0	0.0	0.4	0.0	0.0	M00860 Bacillus anthracis pathogenicity signature, polyglutamic acid capsule biosynthesis
	Drug resistance	0.3	0.3	0.3	0.3	0.3	0.3	0.3	0.3	0.3	0.3	0.3	0.3	M00769 Multidrug resistance, efflux pump MexPQ-OpmE
		0.0	0.3	0.3	0.0	0.3	0.0	0.0	0.3	0.0	0.0	0.0	0.0	M00627 beta-Lactam resistance, Bla system
		0.0	0.3	0.3	0.0	0.0	0.0	0.0	0.0	0.3	0.0	0.3	0.0	M00726 Cationic antimicrobial peptide (CAMP) resistance, lysyl-phosphatidylglycerol (L-PG) synthase MprF
		0.0	0.5	0.5	0.5	0.0	0.5	0.0	0.5	0.5	0.5	0.0	0.0	M00714 Multidrug resistance, efflux pump QacA
Module set	Metabolic capacity	0.5	0.5	0.5	0.0	0.5	0.0	0.5	0.0	0.0	0.0	0.0	0.0	M00611 Oxygenic photosynthesis in plants and cyanobacteria
		1.0	0.5	0.5	0.5	0.5	0.5	0.5	0.0	0.0	0.0	0.0	0.0	M00612 Anoxygenic photosynthesis in purple bacteria
		0.5	0.0	0.0	0.5	0.0	0.5	0.0	0.0	0.0	0.0	0.0	0.0	M00613 Anoxygenic photosynthesis in green nonsulfur bacteria
		0.5	0.5	0.5	0.5	0.5	0.5	0.5	0.5	0.0	0.0	0.5	0.0	M00615 Nitrate assimilation
		0.5	0.5	0.5	0.0	0.5	0.0	0.0	0.0	0.5	0.0	0.5	0.0	M00616 Sulfate-sulfur assimilation
		0.0	0.0	0.0	0.0	0.0	0.0	0.0	0.5	0.0	0.0	0.5	0.5	M00618 Acetogen

Fig. 5 The KEGG annotation diagrams for strains ZM62^T, X9-2-2^T, and 10 closely related taxa in the phylogenetic tree. The numbers in the table represent the completeness of each metabolic step (1 = 100%)

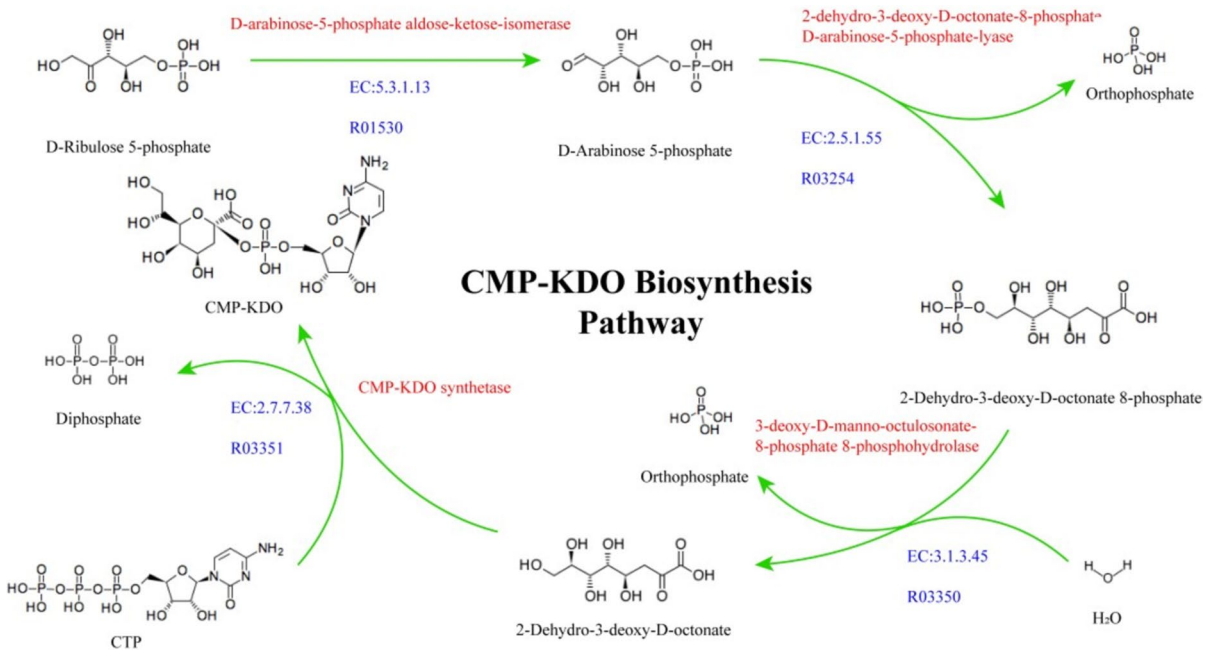

Fig. 6 KEGG annotation indicates that both strains K97^T and NRIC 2002^T possess a complete CMP-KDO biosynthesis pathway. The pathway includes key intermediates and enzymes involved in the conversion from D-ribulose 5-phosphate to CMP-KDO. Green arrows show the reaction flow, red labels indicate enzyme names, and blue text denotes EC numbers and KEGG reaction IDs

PE was also detected in *Z. mangrovi* X9-2-2^T. Phosphatidylethanolamine is a key component of bacterial membranes, and its biosynthesis plays a crucial role in maintaining membrane stability and adaptability, potentially enhancing bacterial survival under environmental stress (Rowlett et al. 2017).

In glycan metabolism, strain ZM62^T shows strong activity in galactofuranan biosynthesis (score = 0.8), a pathway weakly expressed or absent in related taxa ($\leq$0.3; Fig. 6), suggesting a role in cell wall integrity and stress adaptation. It also possesses thiamine and biotin biosynthetic pathways, which are common but moderately active in strain ZM62^T (scores of 0.7 and 0.6, respectively), indicating metabolic versatility that may support survival in nutrient-limited environments.

Strain ZM62^T exhibits potential for terpenoid and polyketide biosynthesis, notably via the dTDP-L-rhamnose pathway. dTDP-L-rhamnose is commonly used to glycosylate secondary metabolites, enhancing their solubility, stability, and biological activity (Thibodeaux et al. 2008; Elshahawi et al. 2015). Genomic analysis revealed that ZM62^T encodes the complete set of enzymes required for dTDP-L-rhamnose biosynthesis, including glucose-1-phosphate thymidylyltransferase (RmlA), dTDP-glucose 4,6-dehydratase (RmlB), dTDP-4-keto-6-deoxyglucose 3,5-epimerase (RmlC), and dTDP-4-keto-L-rhamnose reductase (RmlD). Additionally, several glycosyltransferase genes are located within or adjacent to these biosynthetic gene clusters, suggesting the capacity for producing glycosylated terpenoids or polyketides. This genomic arrangement implies that dTDP-L-rhamnose may play a role not only in metabolite decoration but also in enhancing the structural diversity and bioactivity of the resulting compounds, potentially contributing to ecological interactions, stress adaptation, or antimicrobial activity (Rowlett et al. 2017). From an applied perspective, the capacity of strain ZM62^T to degrade aromatic compounds through the catechol ortho-cleavage pathway (catechol $\rightarrow$ 3-oxoadipate) underscores its potential for xenobiotic biodegradation and environmental remediation (Carmona et al. 2009). Aromatic hydrocarbons are major pollutants in industrial waste and petroleum-derived contaminants, and the presence of this pathway suggests that strain

ZM62^T could be useful in bioremediation efforts. By breaking down these toxic compounds into less harmful intermediates, it may contribute to environmental detoxification and sustainable waste management.

In summary, strain ZM62^T displays a metabolically versatile genome with pathways for processing carbohydrates, amino acids, sulfur compounds, and aromatic compounds. These features suggest ecological adaptability and potential functional roles in organic matter transformation. However, further experimental validation is needed to confirm its capabilities and assess their relevance for environmental or biotechnological applications.

Chemotaxonomic characteristics

The main fatty acid of strain K97^T is Summed Feature 8 ($C_{18:1}\omega6c$/$C_{18:1}\omega7c$), which accounts for 75.73% of the total fatty acid content, followed by $C_{16:0}$, and $C_{18:0}$. The respiratory quinone is Q-10. The major polar lipids of strain K97^T are diphosphatidylglycerol (DPG), phosphatidylethanolamine (PE), and phosphatidylglycerol (PG), which are consistent with those described for the genus *Phycobacter* (Coe et al. 2023). Based on phenotypic characteristics and phylogenetic inferences from 16S rRNA gene and genome sequences, strain K97^T is classified as a new species of the genus *Phycobacter*, for which the name *Phycobacter sedimenti* sp. nov. is proposed. The main fatty acids of strain ZM62^T are Summed Feature 8 ($C_{18:1}\omega6c$/$C_{18:1}\omega7c$), $C_{17:0}$, and $C_{17:1}\omega8c$, accounting for 47.29%, 19.31%, and 4.14%, respectively. The respiratory quinone is Q-10. The major polar lipids of strain ZM62^T are diphosphatidylglycerol (DPG), phosphatidylglycerol (PG), phosphatidylethanolamine (PE), phosphatidylcholine (PC), which are consistent with those described for the genus *Zhengella*. Based on phenotypic characteristics and phylogenetic inferences from 16S rRNA gene and genome sequences, strain ZM62^T is classified as a new species of the genus *Zhengella* for which the name *Zhengella sedimenti* sp. nov. is proposed.

Description of *Phycobacter sedimenti* sp. nov.

Phycobacter sedimenti (se.di.men'ti. L. gen. neut. n. sedimenti, of sediment, from where the type strain was isolated).

Cells are aerobic, Gram-stain-negative, motile short rods, approximately 1.03–1.95 μm in length and 0.41–0.55 μm in width. Colonies are creamy and convex after 4 days of incubation on MA medium. Growth occurs at 20–40 °C (optimum, 33–35 °C), pH 5.5–9.5 (optimum, pH 7.0–8.5), and in the presence of 0.5–7.0% (w/v) NaCl (optimum, 2.0% NaCl). Oxidase, alkaline phosphatase, esterase (C4), esterase lipase (C8), leucine arylamidase, and naphthol-AS-BI-phosphohydrolase activities are positive. Acid is produced from D-ribose, D-tagatose, and 5-keto-D-gluconate potassium. The strain is able to metabolize arginine, ornithine, tryptophan (TDA), and gelatin, as confirmed by API 20E tests. In carbon source oxidation tests, growth is observed with D-trehalose, D-turanose, glucuronamide, tetrazolium violet, L-lactic acid, α-ketoglutaric acid, acetoacetic acid, and acetic acid as sole carbon sources (Table S1). The genomic DNA G+C content is 61.71 mol%. The major respiratory quinone is Q-10. The major fatty acids are Summed Feature 8 ($C_{18:1}\omega6c$/$C_{18:1}\omega7c$), $C_{16:0}$, and $C_{18:0}$. The predominant polar lipids are diphosphatidylglycerol (DPG), phosphatidylethanolamine (PE), and phosphatidylglycerol (PG).

The type strain is K97^T (=KCTC 8365^T=MCCC 1H01460^T), from sediment samples collected from the coast of Xiaoshi Island, Weihai, China (122°0′27.59″ E, 37°31′37.52″ N). The GenBank accession number for the 16S rRNA gene sequence is PP856382 and the draft genome sequence has been deposited in GenBank under the accession number JBBVGR000000000.

Description of *Zhengella sedimenti* sp. nov.

Zhengella sedimenti (se.di.men'ti. L. gen. neut. n. sedimenti, of sediment, from where the type strain was isolated).

Cells are aerobic, Gram-stain-negative, rods, approximately 2.0–4.0 μm in length and 1.0–1.5 μm in width. Colonies are creamy and circular after 4 days of growth on MA medium. Growth occurs at 20–37 °C (optimum, 30–35 °C), pH 5.5–8.5 (optimum, pH 7.5), and in the presence of 0–8.0% (w/v) NaCl (optimum, 2.0% NaCl). The DNA G+C content is 64.76 mol%. The major respiratory quinone is Q-10. The major cellular fatty acids are Summed Feature 8 ($C_{18:1}\omega6c$/$C_{18:1}\omega7c$), $C_{17:0}$, and $C_{17:1}\omega8c$. The predominant polar lipids are diphosphatidylglycerol

(DPG), phosphatidylglycerol (PG), phosphatidylethanolamine (PE), and phosphatidylcholine (PC). Strain ZM62^T is positive for alkaline phosphatase, esterase (C4), leucine arylamidase, valine arylamidase, cystine arylamidase, trypsin, and acid phosphatase (API ZYM). It hydrolyzes gelatin (API 20E). Acid is produced from D-ribose, D-fructose, L-sorbose, and D-tagatose (API 50CH). In Biolog GEN III carbon source utilization tests, growth is observed with dextrin, D-trehalose, D-cellobiose, α-D-glucose, D-galactose, D-fructose-6-phosphate, and glucuronamide (Table S1).

The type strain is ZM62^T (= KCTC 8813^T = MCCC 1H01495^T), from sediment samples collected from the intertidal zone sediments at Jingzi Wharf, Weihai, China (122°0′57.25″ E, 37°31′34.74″ N). The GenBank accession number for the 16S rRNA gene sequence is PQ816740 and the draft genome sequence has been deposited in GenBank under the accession number JBKFFP000000000.

Data summary

All supporting data are provided either within the article or in the supplementary materials.

Acknowledgements We thank Professor Naoto Tanaka at the NRIC (Tokyo University of Agriculture, Japan) for kindly providing the type strain F10T of Phycobacter azelaicus.

Author contributions PRL and JYDL: isolated the strain K97T and ZM62T, analyse most of the data. PRL, JYDL, HZZ, TYL and DCL: performed the experiment. The initial draft of the paper was written by PRL. DCL and ZJD: conceived of the study, designed the study, critically revised the manuscript and co-corresponding the study. All authors read, discussed the results and revised the manuscript.

Funding This work was supported by the Science and Technology Fundamental Resources Investigation Program (Grant Number 2022FY101100), the National Natural Science Foundation of China (92351301) and the Science Foundation for Youths of Shandong Province (ZR2023QC197).

Data availability The type strain K97 (K97^T = KCTC 8365^T = MCCC 1H01437^T) has its 16S rRNA gene sequence available in GenBank under the accession number PP856382, and its draft genome sequence is deposited under the accession number JBBVGR000000000. The type strain ZM62 (ZM62^T = KCTC 8813^T = MCCC 1H01495^T) has its 16S rRNA gene sequence available in GenBank under the accession number PQ816740, and its draft genome sequence is deposited under the accession number JBKFFP000000000.

Declarations

Competing interests The authors declare no competing interests.

Ethical approval This article does not contain any study with human participants or animal experiments by any of the authors.

References

Altschul SF, Gish W, Miller W, Myers EW, Lipman DJ (1990) Basic local alignment search tool. J Mol Biol 215(3):403–410. https://doi.org/10.1016/S0022-2836(05)80360-2

Aramaki T, Blanc-Mathieu R, Endo H, Ohkubo K, Kanehisa M, Goto S, Ogata H (2020) KofamKOALA: KEGG Ortholog assignment based on profile HMM and adaptive score threshold. Bioinformatics 36(7):2251–2252. https://doi.org/10.1093/bioinformatics/btz859

Bertelli C, Brinkman FSL (2018) Improved genomic island predictions with IslandPath-DIMOB. Bioinformatics 34(13):2161–2167. https://doi.org/10.1093/bioinformatics/bty095

Bowman JP (2000) Description of *Cellulophaga algicola* sp. nov., isolated from the surfaces of Antarctic algae, and reclassification of *Cytophaga uliginosa* (ZoBell and Upham 1944) Reichenbach 1989 as *Cellulophaga uliginosa* comb. nov. Int J Syst Evol Microbiol 50:1861–1868. https://doi.org/10.1099/00207713-50-5-1861

Buchfink B, Xie C, Huson DH (2015) Fast and sensitive protein alignment using DIAMOND. Nat Methods 12(1):59–60. https://doi.org/10.1038/nmeth.3176

Cantarel BL, Coutinho PM, Rancurel C, Bernard T, Lombard V, Henrissat B (2009) The carbohydrate-active enzymes database (CAZy): an expert resource for glycogenomics. Nucleic Acids Res 37(Database issue):D233–D238. https://doi.org/10.1093/nar/gkn663

Carmona M, Zamarro María T, Blázquez B, Durante-Rodríguez G, Juárez Javier F, Valderrama JA, Barragán María JL, García José L, Díaz E (2009) Anaerobic catabolism of aromatic compounds: a genetic and genomic view. Microbiol Mol Biol Rev 73(1):71–133. https://doi.org/10.1128/mmbr.00021-08

Coe LSY, Fei C, Weston J, Amin SA (2023) *Phycobacter azelaicus* gen. nov. sp. Nov., a diatom symbiont isolated from the phycosphere of *Asterionellopsis glacialis*. Int J Syst Evol Microbiol 73:10. https://doi.org/10.1099/ijsem.0.006104

Curson ARJ, Todd JD, Sullivan MJ, Johnston AWB (2011) Catabolism of dimethylsulphoniopropionate: microorganisms, enzymes and genes. Nat Rev Microbiol 9(12):849–859. https://doi.org/10.1038/nrmicro2653

Drouillard S, Mine T, Kajiwara H, Yamamoto T, Samain E (2010) Efficient synthesis of 6′-sialyllactose, 6,6′-disialyllactose, and 6′-KDO-lactose by metabolically engineered *E. coli* expressing a multifunctional sialyltransferase from the *Photobacterium* sp. JT-ISH-224. Carbohydr Res 345(10):1394–1399. https://doi.org/10.1016/j.carres.2010.02.018

Elshahawi SI, Shaaban KA, Kharel MK, Thorson JS (2015) A comprehensive review of glycosylated bacterial natural products. Chem Soc Rev 44(21):7591–7697. https://doi.org/10.1039/c4cs00426d

Falkenby LG, Szymanska M, Holkenbrink C, Habicht KS, Andersen JS, Miller M, Frigaard NU (2011) Quantitative proteomics of Chlorobaculum tepidum: insights into the sulfur metabolism of a phototrophic green sulfur bacterium. FEMS Microbiol Lett 323(2):142–150. https://doi.org/10.1111/j.1574-6968.2011.02370.x

Fei C, Ochsenkühn MA, Shibl AA, Isaac A, Wang CH, Amin SA (2020) Quorum sensing regulates "swim-or-stick" lifestyle in the phycosphere. Environ Microbiol 22(11):4761–4778. https://doi.org/10.1111/1462-2920.15228

Felsenstein J (1985) Confidence-limits on phylogenies—an approach using the bootstrap. Evolution 39(4):783–791. https://doi.org/10.2307/2408678

Galperin MY, Makarova KS, Wolf YI, Koonin EV (2015) Expanded microbial genome coverage and improved protein family annotation in the COG database. Nucleic Acids Res 43(D1):D261–D269. https://doi.org/10.1093/nar/gku1223

Huang Z, Guo F, Lai Q, Shao Z (2017) Notoacmeibacter marinus gen. nov., sp. Nov., isolated from the gut of a limpet and proposal of Notoacmeibacteraceae fam. Nov. in the order Rhizobiales of the class Alphaproteobacteria. Int J Syst Evol Microbiol 67(8):2527–2531. https://doi.org/10.1099/ijsem.0.001951

Jansen M, Hansen TA (1997) Tetrahydrofolate serves as a methyl acceptor in the demethylation of dimethylsulfoniopropionate in cell extracts of sulfate-reducing bacteria. Arch Microbiol 169(1):84–87. https://doi.org/10.1007/s002030050545

Konstantinidis KT (2014) Bypassing cultivation to identify bacterial species

Kroppenstedt RM (1982) Separation of bacterial menaquinones by hplc using reverse phase (rp18) and a silver loaded ion-exchanger as stationary phases. J Liq Chromatogr 5(12):2359–2367. https://doi.org/10.1080/01483918208067640

Kumar S, Stecher G, Li M, Knyaz C, Tamura K (2018) MEGA X: molecular evolutionary genetics analysis across computing platforms. Mol Biol Evol 35(6):1547–1549. https://doi.org/10.1093/molbev/msy096/4990887

Lee I, Chalita M, Ha SM, Na SI, Yoon SH, Chun J (2017) ContEst16S: an algorithm that identifies contaminated prokaryotic genomes using 16S RNA gene sequences. Int J Syst Evol Microbiol 67(6):2053–2057. https://doi.org/10.1099/ijsem.0.001872

Li R, Li Y, Kristiansen K, Wang J (2008) SOAP: short oligonucleotide alignment program. Bioinformatics 24(5):713–714. https://doi.org/10.1093/bioinformatics/btn025

Li S, Chen F, Li Y, Wang L, Li H, Gu G, Li E (2022) Rhamnose-containing compounds: biosynthesis and applications. Molecules 27(16):5315

Liang KYH, Orata FD, Boucher YF, Case RJ (2021) Roseobacters in a sea of poly- and paraphyly: whole genome-based taxonomy of the family *Rhodobacteraceae* and the proposal for the split of the "*Roseobacter Clade*" into a novel family, *Roseobacteraceae* fam. nov. Front Microbiol. https://doi.org/10.3389/fmicb.2021.683109

Liao H, Li Y, Lin X, Lai Q, Tian Y (2018) Zhengella mangrovi gen. nov., sp. Nov., a novel member of family Phyllobacteriaceae isolated from mangrove sediment. Int J Syst Evol Microbiol 68(9):2819–2825. https://doi.org/10.1099/ijsem.0.002900

Lin SH, Liao YC (2013) CISA: contig integrator for sequence assembly of bacterial genomes. PLoS ONE 8(3):e60843. https://doi.org/10.1371/journal.pone.0060843

Martens-Uzunova ES, Schaap PJ (2008) An evolutionary conserved d-galacturonic acid metabolic pathway operates across filamentous fungi capable of pectin degradation. Fungal Genet Biol FG & B 45(11):1449–1457. https://doi.org/10.1016/j.fgb.2008.08.002

Meier-Kolthoff JP, Auch AF, Klenk H-P, Göker M (2013) Genome sequence-based species delimitation with confidence intervals and improved distance functions. BMC Bioinform 14(1):60. https://doi.org/10.1186/1471-2105-14-60

Minnikin DE, Odonnell AG, Goodfellow M, Alderson G, Athalye M, Schaal A, Parlett JH (1984) An integrated procedure for the extraction of bacterial isoprenoid quinones and polar lipids. J Microbiol Methods 2(5):233–241. https://doi.org/10.1016/0167-7012(84)90018-6

Patel JB, Tenover FC, Turnidge JD, Jorgensen JH (2011) Susceptibility Test methods: dilution and disk diffusion methods. In: Manual of clinical microbiology, pp 1122–1143. https://doi.org/10.1128/9781555817381.ch71

Pitcher RS, Watmough NJ (2004) The bacterial cytochrome cbb3 oxidases. Biochem Biophys Acta 1655(1–3):388–399. https://doi.org/10.1016/j.bbabio.2003.09.017

Ray PH, Benedict CD (1980) Purification and characterization of specific 3-deoxy-D-manno-octulosonate 8-phosphate phosphatase from Escherichia coli B. J Bacteriol 142(1):60–68. https://doi.org/10.1128/jb.142.1.60-68.1980

Richter M, Rosselló-Móra R, Glöckner FO, Peplies J (2016) JSpeciesWS: a web server for prokaryotic species circumscription based on pairwise genome comparison. Bioinformatics 32(6):929–931. https://doi.org/10.1093/bioinformatics/btv681

Rowlett VW, Mallampalli V, Karlstaedt A, Dowhan W, Taegtmeyer H, Margolin W, Vitrac H (2017) Impact of membrane phospholipid alterations in Escherichia coli on cellular function and bacterial stress adaptation. J Bacteriol. https://doi.org/10.1128/jb.00849-16

Rzhetsky A, Nei M (1992) A simple method for estimating and testing minimum-evolution trees. Mol Biol Evol 9:945–945

Saier MH Jr, Reddy VS, Tsu BV, Ahmed MS, Li C, Moreno-Hagelsieb G (2016) The Transporter Classification Database (TCDB): recent advances. Nucleic Acids Res 44(D1):D372–D379. https://doi.org/10.1093/nar/gkv1103

Saitou N, Nei M (1987) The neighbor-joining method—a new method for reconstructing phylogenetic trees. Mol Biol Evol 4(4):406–425. https://doi.org/10.1093/oxfordjournals.molbev.a040454

Schaefer AL, Greenberg EP, Oliver CM, Oda Y, Huang JJ, Bittan-Banin G, Peres CM, Schmidt S, Juhaszova K, Sufrin JR, Harwood CS (2008) A new class of homoserine lactone quorum-sensing signals. Nature 454(7204):595-U596. https://doi.org/10.1038/nature07088

Shibl AA, Isaac A, Ochsenkühn MA, Cárdenas A, Fei C, Behringer G, Arnoux M, Drou N, Santos MP, Gunsalus KC, Voolstra CR, Amin SA (2020) Diatom modulation of select bacteria through use of two unique secondary metabolites. Proc Natl Acad Sci USA 117(44):27445–27455. https://doi.org/10.1073/pnas.2012088117

Simpson JT, Wong K, Jackman SD, Schein JE, Jones SJ, Birol I (2009) ABySS: a parallel assembler for short read sequence data. Genome Res 19(6):1117–1123. https://doi.org/10.1101/gr.089532.108

Sugai T, Lin C-H, Shen G-J, Wong C-H (1995) CMP-KDO synthetase: overproduction and application to the synthesis of CMP-KDO and analogs. Bioorg Med Chem 3(3):313–320. https://doi.org/10.1016/0968-0896(95)00023-A

Thibodeaux CJ, Melançon CE 3rd, Liu HW (2008) Natural-product sugar biosynthesis and enzymatic glycodiversification. Angew Chem Int Ed Engl 47(51):9814–9859. https://doi.org/10.1002/anie.200801204

Thomas RH (2001) Molecular evolution and phylogenetics. Heredity 86(3):385–385. https://doi.org/10.1046/j.1365-2540.2001.0923a.x

Tindall BJ, Sikorski J, Smibert RA, Krieg NR (2007) Phenotypic characterization and the principles of comparative systematics. In: Methods for general and molecular microbiology, pp 330–393. https://doi.org/10.1128/9781555817497.ch15

Trifinopoulos J, Nguyen LT, von Haeseler A, Minh BQ (2016) W-IQ-TREE: a fast online phylogenetic tool for maximum likelihood analysis. Nucleic Acids Res 44(W1):W232–W235. https://doi.org/10.1093/nar/gkw256

Tsujimoto H, Gotoh N, Nishino T (1999) Diffusion of macrolide antibiotics through the outer membrane of Moraxella catarrhalis. J Infect Chemother 5(4):196–200. https://doi.org/10.1007/s101560050034

Urban M, Cuzick A, Seager J, Wood V, Rutherford K, Venkatesh SY, De Silva N, Martinez MC, Pedro H, Yates AD, Hassani-Pak K, Hammond-Kosack KE (2020) PHI-base: the pathogen-host interactions database. Nucleic Acids Res 48(D1):D613-d620. https://doi.org/10.1093/nar/gkz904

Weisburg WG, Barns SM, Pelletier DA, Lane DJ (1991) 16S ribosomal DNA amplification for phylogenetic study. J Bacteriol 173(2):697–703. https://doi.org/10.1128/jb.173.2.697-703.1991

Wu B, Liu F, Fang W, Yang T, Chen G-H, He Z, Wang S (2021) Microbial sulfur metabolism and environmental implications. Sci Total Environ 778:146085. https://doi.org/10.1016/j.scitotenv.2021.146085

Xie J, Chen Y, Cai G, Cai R, Hu Z, Wang H (2023) Tree visualization by one table (tvBOT): a web application for visualizing, modifying and annotating phylogenetic trees. Nucleic Acids Res 51(W1):W587–W592. https://doi.org/10.1093/nar/gkad359

Xu XW, Wu YH, Wang CS, Oren A, Zhou PJ, Wu M (2007) *Haloferax larsenii* sp. nov., an extremely halophilic archaeon from a solar saltern. Int J Syst Evol Microbiol 57:717–720. https://doi.org/10.1099/ijs.0.64573-0

Yew Wen S, Gerlt John A (2002) Utilization of l-ascorbate by Escherichia coli K-12: assignments of functions to products of the yjf-sga and yia-sgb Operons. J Bacteriol 184(1):302–306. https://doi.org/10.1128/jb.184.1.302-306.2002

Yoon S-H, Ha S-m, Lim J, Kwon S, Chun J (2017a) A large-scale evaluation of algorithms to calculate average nucleotide identity. Antonie Van Leeuwenhoek 110(10):1281–1286. https://doi.org/10.1007/s10482-017-0844-4

Yoon SH, Ha SM, Kwon S, Lim J, Kim Y, Seo H, Chun J (2017b) Introducing EzBioCloud: a taxonomically united database of 16S rRNA gene sequences and whole-genome assemblies. Int J Syst Evol Microbiol 67(5):1613–1617. https://doi.org/10.1099/ijsem.0.001755

Zhang G, Meredith TC, Kahne D (2013) On the essentiality of lipopolysaccharide to gram-negative bacteria. Curr Opin Microbiol 16(6):779–785. https://doi.org/10.1016/j.mib.2013.09.007

Zhu Y, Thomas F, Larocque R, Li N, Duffieux D, Cladière L, Souchaud F, Michel G, McBride MJ (2017) Genetic analyses unravel the crucial role of a horizontally acquired alginate lyase for brown algal biomass degradation by Zobellia galactanivorans. Environ Microbiol 19(6):2164–2181. https://doi.org/10.1111/1462-2920.13699